[10] Carriere, P. and Sirieix, M., "Facteurs d'Influence du Receullement d'un Ecoulement Supersonique," *Proceedings of the 10th International Congress of Applied Mechanics*, Stresa, Italy, 1960.

[11] McDonald, H., "An Analysis of the Turbulent Base Pressure Problem in Supersonic Axisymmetric Flow," *The Aeronautical Quarterly*, Vol. XVI, May 1965, pp. 97–121.

[12] Korst, H. H., Chow, W. L. and Zumwalt, G. W., "Research on Transonic and Supersonic Flow of a Real Fluid at Abrupt Increases in Cross Section (With Special Consideration of Base Drag Problems)," ME TR 392-5, Oct. 1964, University of Illinois, Urbana, Ill.

[13] McDonald H. and Hughs, P. F., "A Correlation of High Subsonic Afterbody Drag in the Presence of a Propulsive Jet or Support Sting," *Journal of Aircraft*, Vol. 2, No. 3, May–June, 1965, pp. 202–207.

[14] Dixon, R. J. and Page, R. H., "Interdependence of Base Pressure and Base Heat Transfer," *ARS Journal*, Vol. 31, No. 12, Dec. 1961, pp. 1785–1786.

[15] Collines, D. J., Lees, L. and Roshko, A., "Near Wake of a Hypersonic Blunt Body with Mass Additions," *AIAA Journal*, Vol. 8, No. 5, May 1970, pp. 833–842.

[16] Mueller, T. J., United Aircraft Research Laboratory, East Hartford, Conn. 1965, unpublished data.

MAY 1972 J. SPACECRAFT VOL. 9, NO. 5

Material Phase Transformation Effects upon Performance of Spaced Bumper Systems

A. K. HOPKINS*
Air Force Materials Laboratory, Wright-Patterson Air Force Base, Ohio

T. W. LEE† AND H. F. SWIFT‡
University of Dayton Research Institute, Dayton, Ohio

The response of thin metal sheets to impacts by spheres of like materials in the entire velocity range to 7.2 km/sec is considered. Regimes of impact are observed characterized first by the projectile remaining intact, thence to projectile shatter, to melting of sphere and plate, and finally to vaporization of the materials. The thickness of witness plate material required to defeat the forward moving debris created by the thin plate impact is shown to depend on the physical state of the debris material. An analysis based upon planar shock wave theory is shown to accurately predict critical points on the ballistic limit curve associated with both incipient and complete melting and vaporization of the projectile and target materials.

Nomenclature

A, γ = coefficient and exponent for Murnaghan equation
E_H, P_H, V_H = Hugoniot energy, pressure, volume
E_0, V_0 = normal energy, volume
i = ith state or point
P^* = maximum shock pressure
s = spacing, cm
S = entropy, cal/°K
t_1, t_2 = thickness, cm
T = absolute temperature, °K
u_p = particle velocity in projectile, cm/μsec
u_T = particle velocity in target, cm/μsec
V^* = minimum volume
V_f = final volume, cm^3/g
v_0, v = impact velocity, km/sec
Γ = Grüneisen parameter

Introduction and Background

AS early as 1947, Whipple[1] suggested that the most efficient method of defeating the penetrating power of a meteorite into the surface of a space vehicle is to provide the surface with a bumper. In his book published in 1958, Whipple[2] discusses the bumper concept in some detail, suggesting that over-all hull weight might be dramatically reduced by using the bumper concept.

Researchers since 1958 have developed the space bumper concept and have sought theoretical models which would explain the reason the bumper was effective and predict results of real impacts in space. In 1964 Maiden and McMillan[3] described the failure modes of bumper configurations at low and high velocity and suggested a one-dimensional analysis that would aid a space craft designer to estimate the bumper parameter values he would need in the construction of his vehicle.

In 1970, Swift and Hopkins[4] reported the effects of bumper materials upon the performance of two-component hypervelocity impact shields. They noted that most bumper materials performed equally well on a weight-per-unit-area basis, i.e., bumper areal density was the only factor controlling shield performance. This rule held exactly when one-dimensional shock wave analysis indicated that the projectiles (aluminum spheres) were melted by the primary shock wave and the bumper material also melted. Small deviations from the areal density rule were observed when the projectile melted, but the bumper material was neither vaporized nor shattered but left in the solid state. Shield performance degraded dramatically when the shock impedance of the bumper materials was insufficient to generate shock waves in the projectile strong enough to melt the projectile material—thus leaving the projectile material shattered but in the solid state. The authors hypothesized that the critical shock impedance of the bumper material needed to assure validity of

Received November 23, 1971; revision received January 18, 1972.
* Research Physicist.
† Head, Impact Physics Group.
‡ Head, Materials Physics Research.

the areal density rule is dependent upon projectile impact velocity. This dependence involves the generation of shock waves in the projectile of sufficient intensity to assure material melting.

Nysmith[5] very excellently described the type of damage to the hull plate by the debris from the bumper impact, and discussed the physical processes by which the hull plate fails. He pointed out that a ballistic limit curve of the hull plate may have several peaks depending on the state of the material in the debris cloud and the distance separating the bumper and hull plate.

Experimental Design and Results

The experiment described below was devised to learn more about the role of shock heating in determining the performance of two-element hypervelocity impact shields. Specifically, the hypothesis of Swift and Hopkins concerning projectile melting is investigated, and its more general validity is examined by applying it to a situation involving projectile vaporization. The geometry shown in Fig. 1 is used to examine the damage on the hull plate behind a bumper as a function of impact velocity. The spacing s was held constant at 5.08 cm; the projectile diameter d was 3.17 mm, and bumper thickness t_1 was held constant at 0.787 mm.

In this series of tests the second, or hull, plate was used as the indicator in all cases. The hull plate, type 6061-T6 aluminum, was varied in thickness at a given velocity to determine a ballistic limit thickness. The ballistic limit was defined as a line between puncture and nonpuncture. Several criteria were used to determine when puncture had been achieved if the hole was not obvious: one was that no dye penetrant would show on the reverse side; another was that no gas should leak through the plate. In general, the gas leak criterion was used on questionable penetrations.

Two materials were used for the impacting projectile and the bumper plate. In the first case, 3.17-mm aluminum spheres were impacted against 0.787-mm-thick 6061-T6 aluminum plates. In the second case, 3.17-mm cadmium spheres impacted 0.787-mm-thick cadmium plates. Aluminum was chosen for the experiment because, in addition to being a common structural material, it has been carefully studied and its hydrodynamic properties are well known. The cadmium was chosen for comparison because the energies required for melting and vaporization are small compared to other structural metals.

Figure 2 shows the experimental results. The solid line represents the best estimate of the ballistic limit for aluminum, the dashed line for cadmium. The data was subject to some scatter because of the statistical nature of the debris material. The points marked by arrows are from the theory discussed later. Figures 3 and 4 are photographs of typical damage to the hull plate at the velocities shown. Figure 3 shows damage behind an aluminum bumper, Fig. 4 behind a cadmium bumper.

Each curve in Fig. 2 has an additional peak at velocities above the traditional peak normally ascribed to material shatter. To effectively describe the types of damage seen in the photographs of Fig. 3 and Fig. 4, it is convenient to draw a

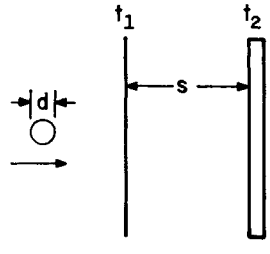

Fig. 1 Experimental configuration showing the projectile, bumper, and witness plate positions.

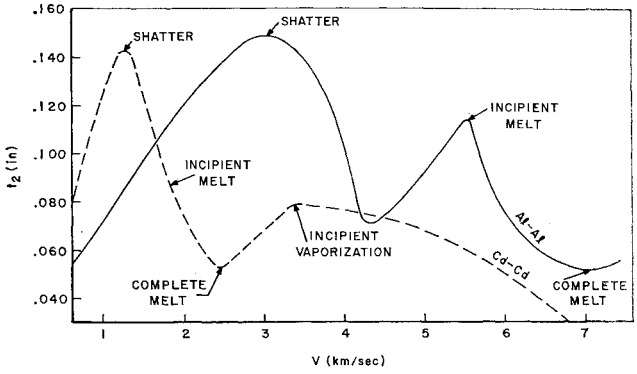

Fig. 2 Ballistic limit curves; t_2 is the thickness of the witness plate.

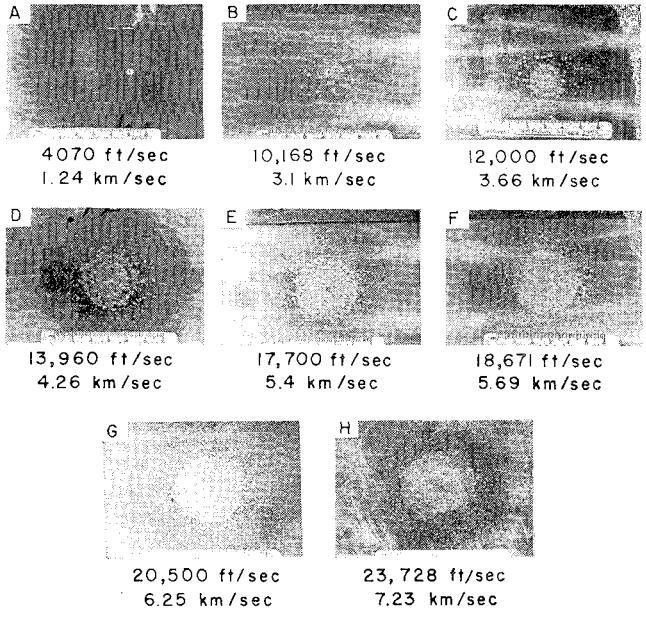

Fig. 3 Witness plates for the aluminum impact case, showing the changing debris character and pattern.

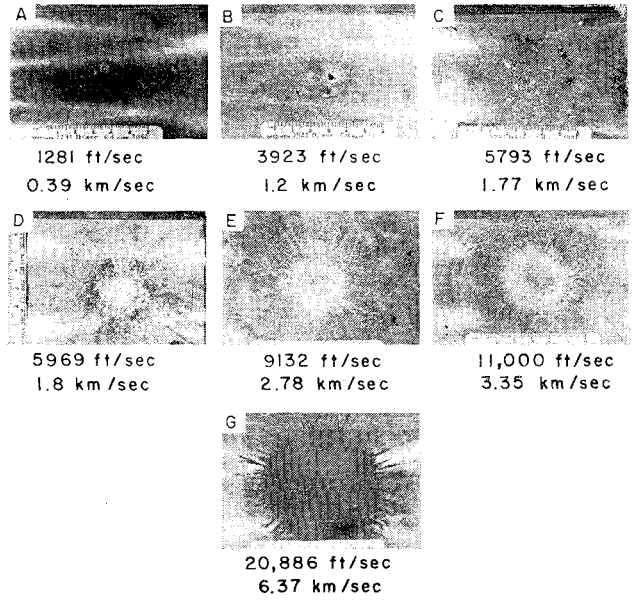

Fig. 4 Witness plates for the cadmium impact case, showing the changing debris character and pattern.

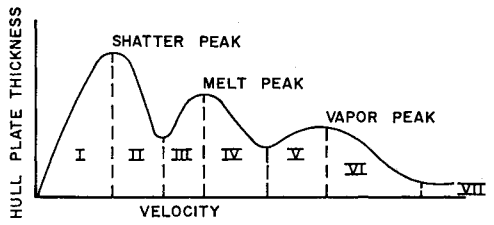

Fig. 5 Schematic composite ballistic limit curve showing the debris character regions described in the text.

composite ballistic limit curve shown in Fig. 5. The hull plate damage can be described in terms of the damage characteristic to the various regions marked in Fig. 5.

Typical damage in region I is a single crater on the hull plate. The projectile passes through the bumper suffering only a loss in velocity and impacts the hull plate completely intact. Figures 3A and 4A are examples of Region I damage. Typical damage in region II is a graduation from a few fairly large craters indicating the projectile break-up to a multitude of very small craters indicating the projectile and bumper were badly shattered. The damage on the hull plate in region III retains a rather constant appearance throughout, with each tiny crater becoming larger and deeper as the velocity increases.

At transition between region III and region IV the damage begins to take on a new appearance. The many tiny craters made by solid particles are interspersed with soft contour craters made by liquid droplets. The change in damage character can be seen by comparing Figs. 3E and 3F and by comparing Figs. 4C and 4D. Throughout region IV the ratio of liquid impact to solid impact increases with velocity until complete melt is achieved. Complete melt is barely reached in the Al-Al impact as is seen in Fig. 3H. It is interesting to note that region III does not exist in the Cd-Cd impact situation because incipient melt is achieved before complete shatter is accomplished. The hull plate damage then goes directly from that characteristic of region II to that of region IV. Damage typical of region IV is seen in Figs. 3G and 4E. The damage on the hull plate throughout region V is that of liquid droplet impacts. Figures 3H and 4F are examples of region V damage.

Region VI is characterized by a mixture of liquid and vapor damage. The vapor peak at the transition from region V to region VI occurs at incipient vaporization where the damage mechanism changes from cratering to pressing by high-pressure gas. Late in region VI and throughout region VII the failure mode is by rupture and tearing rather than by penetration and perforation. Figure 4G is typical of region VII damage.

Discussion

The various peaks in the ballistic limit curves have been attributed to the changes in either the mechanical or the physical state of the debris cloud generated at impact behind the bumper. The cloud consists of the projectile and bumper material driven forward at impact. The first peak was associated with projectile breakup, the second with melting, and the third with vaporization. The authors are not aware of any analytical techniques which will predict the velocity at which projectile fragmentation will occur.

The analytical tools for predicting the changes in physical state are well in hand and will be outlined here. Assuming the colliding bodies are planar, a relatively straightforward one-dimensional planar shock wave analysis may be applied. The competing processes of shock amplification by focusing, shock decay by rarefactions, and mechanical working, all of which are nonplanar shock effects, appear (from the data) to have cancelling effects and thus are neglected in this analysis.

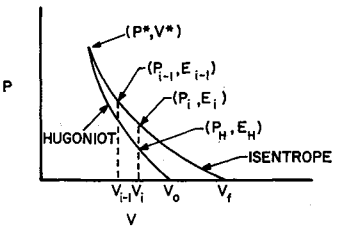

Fig. 6 Schematic shock Hugoniot-release isentrope plot showing calculation scheme described in the text.

Consider the pressure/volume plane of the pressure/volume/energy space depicted in Fig. 6. The material is shock compressed along a Rayleigh line (that straight line connecting V_0 with V^*) to some final state which lies on the Hugoniot curve (a locus of end points of states arrived at by a nonisentropic shock process).[6] The release from this shocked state is an isentropic process and thus follows an unloading path indicated in Fig. 6 to some final volume V_f. Since the entropy is increased during the shock process and is constant during release, the final entropy is larger than the initial entropy. The result is an expanded volume final state. As the collision velocity is increased, the target and projectile both experience more shock heating so that upon release, material phase changes may occur in both objects. Again, using a planar shock wave analysis, predictions of the pressure levels behind the shock wave that will cause these phase changes may be made. The phase transition zones are plateaus of constant temperature connecting points of the onset and completion of a phase change in pure materials.

To determine the critical pressures marking the beginning and ending of the mixed phase condition, one must obtain the residual energy after shock compression and subsequent isentropic release. These can be obtained from the shock and release P-V loci. The energy behind the shock wave is determined from the Rankine-Hugoniot equation

$$E_H - E_0 = (P_H/2)(V_0 - V_H) \tag{1}$$

which is derived from the two Hugoniot shock jump conditions describing conservation of mass and momentum. To relate the Hugoniot pressure to volume the Murnaghan[7] incomplete equation of state was chosen:

$$P_H = A[(V_0/V_H)^\gamma - 1] \tag{2}$$

McQueen et al.[8] have developed the following equations which one can use to develop the release isentrope P-V locus shown in Fig. 6.

$$P = \frac{P_H - (\Gamma/V)_i[P_{i-1}\,\Delta V/2 + E_H - E_{i-1}]}{1 + (\Gamma/V)_i\,\Delta V/2} \tag{3}$$

$$E_i = E_{i-1} - [(P_i + P_{i-1})\Delta V/2] \tag{4}$$

These equations are obtained from the combined first and second laws of thermodynamics:

$$dE = TdS - PdV \quad \text{with } dS = 0 \tag{5}$$

and the Grüneisen difference equation:

$$P_i = P_H + (\Gamma/V)_i(E_i - E_H) \tag{6}$$

The energy under the isentrope is found by integrating the P-V locus numerically. Although material phase changes are nonisentropic processes, the work of Asay[9] indicates that release from the shock state is nearly isentropic even when crossing phase lines. This isentropic energy is then subtracted from the Hugoniot energy as calculated by Eq. (1) to yield the residual energy. The internal energy (at atmospheric pressure) for each critical point (the release state of interest is at atmospheric pressure) is available in various publications. The data and equations listed in Wicks and Block[10] were used for aluminum and cadmium. The above calculations were solved iteratively until the residual energy matched the critical energy.

Table 1 Pressures associated with phase change points

		Melt				Vapor			
		Incipient		Complete		Incipient		Complete	
Material	Const	P, Mb	V_0, km/sec	P, Mb	V_0 km/sec	P, Mb	V_0, km/sec	P, Mb	V_0, km/sec
Cd[a]	Γ	0.32	1.86	0.456	2.41	0.746	3.36	4.65[c]	10.4
Cd	Γ/V	0.31	1.82	0.44	2.34	0.701	3.23	7.5[c]	13.8
Al[b]	Γ	0.68	5.62	0.95	7.04	Beyond range of interest			
Al	Γ/V	0.65	5.43	0.89	6.77	Beyond range of interest			

[a] Materials constants: A = 0.0931 Mb, γ = 5.52, Γ = 2.33.
[b] Materials constants: A = 0.1704 Mb, γ = 4.3, Γ = 2.0.
[c] Beyond range of applicability of Murnaghan equation.

The Grüneisen parameter Γ is constant or at most a function of volume during mild compressions. Parallel calculations based upon Γ-const and Γ/V = const were performed. The particle velocity behind the shock wave at the critical pressure is obtained from:

$$u_T = [P^*(V_0 - V^*)]^{1/2}$$

For the cases treated in this report, the projectile and target are the same material so that the boundary condition at the projectile/target interface, $v = u_T + u_p$, reduces to $v = 2u_T$. The results of all these calculations are shown in Table 1.

These critical velocities are indicated in Fig. 2. It is of interest to note the positions of the predicted critical points. In the case of cadmium, the predicted incipient melting stage still lies under the shatter peak, while the complete melt prediction lies in the valley. One might postulate that upon completion of melting, successive additions to the projectile kinetic energy just increase the amount of hull plate material required to completely defeat the projectile. This is seen to be the situation with cadmium until incipient vaporization occurs. The additional kinetic energy gained beyond the incipient-vaporization point is consumed in the phase transformation. Also with the onset of vaporization, the damage mode on the hull plate begins to change and becomes one characterized by a long, low-level stress attributable to a gaseous cloud. A similar description applies to the aluminum case. However, the onset of melting is noted by a distinct peak, and the completion of melting is in the valley.

Conclusions

Although somewhat simplified analytical forms are used here, the data/theory match indicates the validity of the approach. The one-dimensional analysis employed, although incomplete, is sufficiently powerful both to predict the peaks and the valleys of the ballistic limit curve in this velocity interval and to indicate the reason for their existence and location. The authors, therefore, must conclude that whatever other processes operate at impact within the bumper and the projectile, the simple one-dimensional shock compression and isentropic relaxation are dominant.

The one-dimensional analysis predicts the impact velocity for the onset of melting, complete melting, and incipient vaporization in the impact velocity range of the experiment for impacting of like materials. The same type of analysis can be used to predict Hugoniot conditions when different materials impact. The residual temperature upon isentropic relaxation can be calculated for each constituent in impacts of unlike materials. The ballistic limit curve for the hull plate behind such bumper impacts may be complicated by the individual melting and vaporization temperatures of each material. In general, the assumption of Γ = const appears to give the best prediction of critical points on the ballistic limit curve.

References

[1] Whipple, F. L., "Meteorites and Space Travels," *Astronomical Journal*, No. 1161, Feb. 1947, p. 131.

[2] Whipple, F. L., "The Meteoric Risk to Space Vehicles," *Vistas in Astronautics*, Pergamon Press, New York, 1958, pp. 115–124.

[3] Maiden, C. J. and McMillan, A. R., "An Investigation of the Protection Afforded Spacecraft by a Thin Shield," *AIAA Journal*, Vol. 2, No. 11, Nov. 1964, pp. 1922–1998.

[4] Swift, H. F. and Hopkins, A. K., "The Effects of Bumper Material Properties on the Operation of Spaced Meteoroid Shields," *Journal of Spacecraft and Rockets*, Vol. 7, No. 1, Jan. 1970, pp. 73–77.

[5] Nysmith, R. C., "A Discussion of the Modes of Failure of Bumper-Hull Structures with Application to the Meteoroid Hazard," TN D-6039, Oct. 1970, NASA.

[6] Bjork, R. L. and Olshaker, A. E., "The Role of Melting and Vaporization in Hypervelocity Impact," RM-3490-PR, May 1965, The Rand Corp., Santa Monica, Calif.

[7] Gogolev, V. M., Mirkin, V. G., and Yablokova, G. I., "Approximate Equation of State for Solids," *Zhurnal Prikladnoi Mikhaniki i Tekhnukeskoi Fiziki*, Vol. 5, 1963, pp. 93–98.

[8] McQueen, R. G., et al., "Equation of State of Solids," *High Velocity Impact Phenomena*, edited by R. Kinslow, Academic Press, New York, 1970, pp. 297–298.

[9] Asay, J. R., Private communication, Aug. 1971, Sandia Corp., Albuquerque, N. Mex.

[10] Wicks, C. E. and Block, F. E., "Thermodynamic Properties of 65 Elements," U.S. Bureau of Mines Bulletin 605, U.S. Government Printing Office, Washington, D.C., 1963, pp. 10, 24.